LANGMUIR

pubs.acs.org/Langmuir Article

Nitroxide-Modified Silica Nanoparticles: Impact of Radical Density on Relaxometric and EPR Properties

Pierre Ernotte, Amandine Maes, Sarah Garifo, Isalyne Drewek, Yves-Michel Frapart, Robert N. Muller, Dimitri Stanicki,* and Sophie Laurent

Cite This: https://doi.org/10.1021/acs.langmuir.5c01616 Read Online

ABSTRACT: In this study, we report the synthesis and characterization of nitroxide-functionalized silica nanoparticles incorporating a TEMPO-based spin label. These nanoparticles were prepared through a reverse microemulsion method, and the nitroxide moiety was introduced via a TEMPO-modified silane, synthesized by coupling 4-amino-TEMPO with 3-(triethoxysilyl)propylsuccinic anhydride. By adjusting experimental parameters, we successfully modulated the radical surface density, obtaining values ranging from 0.36 to 2.83 radicals/nm^2, as determined by UV spectroscopy. Relaxometric measurements showed that both longitudinal (r_1) and transverse (r_2) relaxivities were strongly influenced by radical density, reaching maximum values of 5.42 and 11.94 $s^{-1}\cdot mM^{-1}$, respectively, corresponding to enhancements of up to 489% (r_1) and 712% (r_2) compared to free 4-amino-TEMPO (at 20 MHz). Interestingly, high surface loading led to a decrease in relaxivity, highlighting the role of spin−spin interactions in modulating the relaxation process. Phantom electron paramagnetic resonance imaging (EPRI) demonstrated improved contrast and resolution for formulations with low radical densities, highlighting the importance of surface engineering to optimize the nanoparticle performance for EPRI applications.

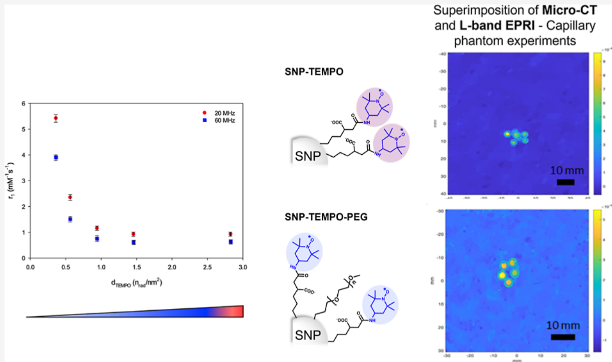

■ INTRODUCTION

Magnetic resonance imaging (MRI) is one of the most widely used imaging methods, which is routinely employed in clinical settings to detect a range of pathologies, including cancers, strokes, and inflammatory conditions. Despite its advantages, the low sensitivity inherent in MRI often requires the use of contrast agents to improve image quality and diagnosis. These agents work by modifying the water proton relaxation times, thereby improving the visibility of certain tissues and facilitating a more accurate diagnosis. Gadolinium-based contrast agents (GBCAs) are among the most commonly used due to their high ^{1}H relaxivity and wide availability. However, concerns about their potential toxicity have emerged in recent years.[1]

Studies have highlighted that repeated administration of GBCAs may be linked to nephrogenic systemic fibrosis and gadolinium accumulation in the brain.[2,3] While macrocyclic gadolinium complexes have been developed to reduce these risks, safety concerns persist, and the development of gadolinium-free contrast agents has become a priority. Among the most studied alternatives are iron oxide nanoparticles (NPs), which exhibit superparamagnetic properties suitable for MRI and avoid the toxicity risks associated with free gadolinium ions.[4,5] Several formulations, such as Endorem (Feridex in the U.S.) and Sinerem, were previously approved for clinical use as liver and lymph node contrast agents, respectively. However, these agents were eventually withdrawn from the market due to limited clinical demand and challenges related to image interpretation and pharmacokinetics.

Nitroxides are another class of compounds of interest consisting of relatively stable organic radicals (under mild conditions). They have been extensively investigated for a variety of applications, ranging from antioxidants[6,7] to spin labeling for electron paramagnetic resonance (EPR).[8] Due to their unpaired electron, nitroxides can potentially be used as contrast agents for MRI. However, compared with GBCAs, their relaxivity is significantly lower, typically ranging from 0.1 to 0.5 $mM^{-1}\cdot s^{-1}$ at 37 °C under high magnetic fields. These low relaxivity values are attributed partly to the presence of a single unpaired electron (compared to 7 for gadolinium) and partly to the fact that relaxation mechanisms of free nitroxide radicals mainly involve outer sphere interactions.[9,10] In addition, it should be mentioned that nitroxide radicals can

Received: April 1, 2025
Revised: July 1, 2025
Accepted: July 2, 2025

be readily reduced by biological reducing agents, such as vitamin C or glutathione (GSH),[11,12] in diamagnetic hydroxylamine, which does not affect water relaxation. Consequently, the contrast generated by nitroxides is transient and can only be observed for a limited period in biological media. Some recent reports have highlighted that nanotechnology-based strategies may appear promising to overcome the limitations of nitroxides. In this context, several types of formulations[13−16] have been investigated, including dendrimers, gold nanorods, micelles, or proteins. Each of these systems has been shown to either significantly enhance nitroxide ^{1}H relaxivity[17−19] and/or improve radical chemical stability. For example, in 2017, H. Nguyen et al.[20] demonstrated that the association of nitroxides with brush-arm star polymers leads to a substantial increase in both transverse relaxivity (reaching 7.40 $mM^{-1}\cdot s^{-1}$) and nitroxide stability. More recently,[21] nitroxide-anchored chitosan NPs have been successfully used to visualize tumors in mice using T_1-weighted MRI.

Among the diverse types of nanosystems, silica NPs (SNPs) are considered one of the most promising classes, garnering increasing interest due to their favorable safety profile,[22,23] including biodegradability and low cytotoxicity, which makes these systems particularly suitable for biomedical applications. Another key advantage of SNPs is their ease of functionalization, as their surface can be readily tailored through silane chemistry to optimize interactions with biological environments and enhance biocompatibility (e.g., polyethylene glycol (PEG) grafting is a common strategy to improve colloidal stability and reduce recognition by the mononuclear phagocyte system). Moreover, a wide variety of compounds can be encapsulated within their cores during synthesis. As a result, SNPs have been extensively explored in imaging applications, especially for improving the contrast performance of existing MRI agents.[24−27]

Given the physicochemical properties of SNPs (notably, their ability to restrict molecular motion and maintain structured hydration layers), the immobilization of nitroxide radicals on such solid supports is expected to modulate key relaxation parameters. In particular, covalent attachment to the NP surface should increase the rotational correlation time of the radicals, while the high surface hydrophilicity of SNPs may foster prolonged interactions with the surrounding water molecules. Both effects are favorable to the above-mentioned outer sphere relaxation mechanisms and support the hypothesis that conjugating nitroxides to SNPs could enhance their relaxometric efficiency.

For these reasons, novel nitroxide-modified SNPs were developed to investigate both proton relaxivity and radical stability, particularly under reducing conditions. The strategy involved anchoring a silane derivative of TEMPO onto the surface of SNPs synthesized via a reverse microemulsion process. By tuning the synthesis parameters, we successfully modulated the surface density of nitroxide groups, which in turn significantly influenced the relaxometric behavior of the resulting NPs. Nitroxide-functionalized NPs have also been identified as promising probes for EPR imaging (EPRI).[28] In this context, their effectiveness was demonstrated through phantom imaging, revealing encouraging results. Importantly, variations in radical surface density were shown to impact image resolution, indicating that fine-tuning this parameter could further enhance the NP performance in EPRI applications.

■ MATERIALS AND METHODS

Materials. Triton X-100, ammonium hydroxide (30−33%), hexan-1-ol, tetraethylorthosilicate (TEOS, 99.9%), and sodium ascorbate were purchased from Sigma-Aldrich (Belgium); cyclohexane (99.9%), acetone (98%), diethyl ether (99%), dichloromethane (99%), ethanol (99%), and amino-TEMPO were purchased from VWR (Belgium); (3-triethoxysilyl)propyl succinic anhydride (TEPSA) was purchased from Gelest Inc. (Morrisville, USA); silanated PEG MW = 1 kDa (Si-PEG_{1k}) was purchased from Biopharma PEG (Watertown, USA). All of the materials mentioned above were used directly, without any further treatment. Stirred cells and membranes for ultrafiltration (MWCO = 100 kDa) were purchased from Merck Millipore (USA). Membranes Spectra/Por (MWCO = 12−14 kDa) for dialysis were acquired from VWR (Belgium).

Methods. *Synthesis of TEPSA−TEMPO.* TEPSA (200 μL, 0.711 mmol) was dissolved in dichloromethane (5 mL), and then amino-TEMPO (122.6 mg, 0.697 mmol) was added. The solution was left under stirring for 4 h, and the reaction was followed by electrospray ionization−mass spectrometry (ESI−MS) until disappearance of the amino-TEMPO signal. The solvent was removed under a vacuum to obtain an orange solid. The crude product was used in the next step without further purification. ESI(+)−MS $[MH]^+$ m/z 478. ^{1}H NMR (500 MHz, D_2O): δ (ppm) 4.14 (m, 1H, a), 3.64 (q, J = 6.9 Hz, 6H, b), 2.59 (m, 2H, c), 2.33−2.17 (m, 1H, d), 2.02 (d, J = 12.9 Hz, 4H, e), 1.92 (s, 2H, f), 1.61 (m, 4H, g + h), 1.22 (m, 15H, i + j), 0.80−0.60 (m, 2H, k) (refer to Figure S2 for peak assignment).

Preparation of TEMPO-Modified SNPs. A water-in-oil (w/o) reversed-phase microemulsion was prepared by mixing cyclohexane (9 mL), hexanol (2 mL), Triton X-100 (2 mL), and deionized water (1 mL) in an amber flask. The mixture was stirred at room temperature for 30 min, after which TEOS (100 μL, 0.45 mmol) was added. After an additional 30 min, NH_4OH (30%, 60 μL) was introduced, and the solution was stirred continuously for 24 h at room temperature. Next, TEOS (50 μL, 0.22 mmol) was added, followed 30 min later by the addition of the organosilane derivative. For the SNP **1.1**−**1.3** batches, only TEPSA−TEMPO was added (32 mg, 0.068 mmol; 25 mg, 0.053 mmol; or 18.5 mg, 0.039 mmol for SNP **1.1**, SNP **1.2**, and SNP **1.3**, respectively). For the SNP **2.1** and **2.2** batches, a co-grafting strategy was employed, using a fixed amount of Si-$mPEG_{1k}$ (20 mg, 0.05 mmol) and varying amounts of TEPSA−TEMPO (18.5 mg, 0.039 mmol and 12 mg, 0.025 mmol for SNP **2.1** and SNP **2.2**, respectively). After an overnight reaction, the particles were precipitated by adding a 1:1 acetone/diethyl ether mixture (20 mL), isolated via centrifugation (10 min at 6000 rpm), and washed twice with ethanol (5 mL). The particles were then redispersed in 2 mL of deionized water, followed by dialysis against deionized water (MWCO = 12−14 kDa) for 3 days at 35 °C. Finally, the solution was concentrated to 1 mL using ultrafiltration.

Characterization Techniques. Dynamic light scattering (DLS) measurements of NP suspensions were performed using a Zetasizer Nano ZS particle size analyzer (He−Ne laser, 633 nm; Malvern Instruments, Worcestershire, UK) on diluted suspensions (1 mg/mL). The mean hydrodynamic diameter size and the polydispersity index (PDI) of particle suspension were measured in aqueous media at 25 °C. Transmission electron microscopy (TEM) images were recorded to determine particle morphological details using a Fei Tecnai 10 microscope (Oregon, USA) working at an operating voltage of 80 kV. Each TEM specimen was prepared using silica suspension (0.1 mg/mL) that was dropped onto 300 mesh carbon-coated Formvar grids from Ted Pella Inc. After slow evaporation of the water in air at room temperature, particles were observed. Statistical analysis was extracted from multiple image examinations of each sample using iTEM software (Münster, Germany). By measuring diameter size over 250 counted NPs for each sample, the mean diameter (D^{TEM}), the PDI (PDI^{TEM}) and a standard deviation from the corresponding particle suspension were calculated.[29]

For practical reasons, the nitroxide concentration was quantified by UV spectroscopy using a Lambda35 UV/vis spectrophotometer (PerkinElmer, USA) with a blank containing nitroxide-free SNPs. The

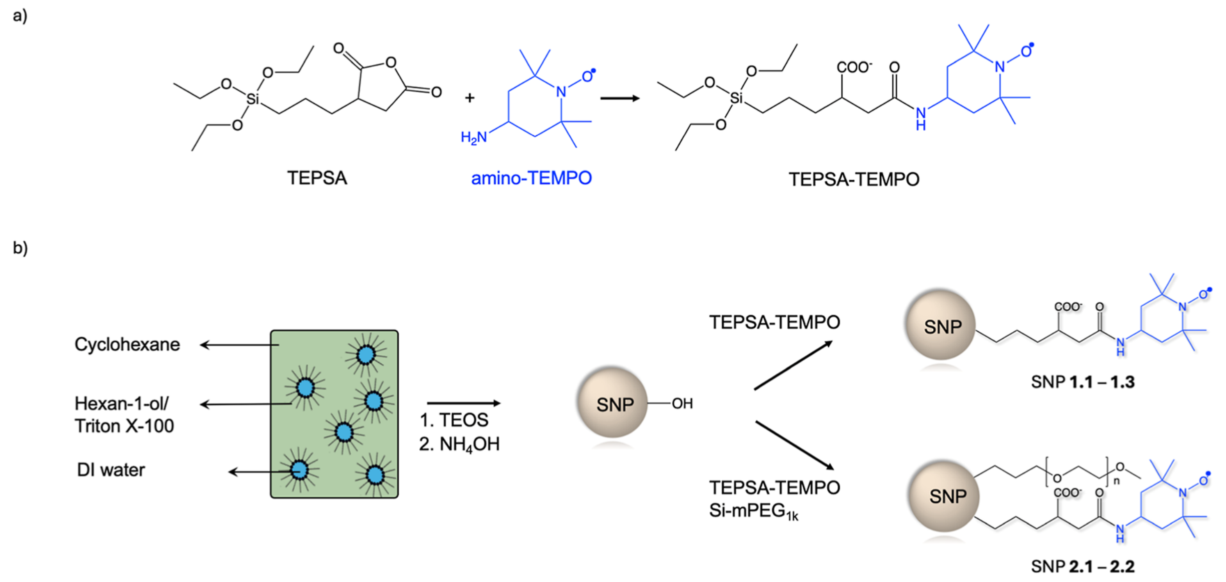

Figure 1. (a) Reaction scheme to obtain the silanized TEMPO derivative (TEPSA–TEMPO); (b) schematic representation of SNP synthesis using the reversed microemulsion method and their surface functionalization with TEPSA–TEMPO (SNP **1.1–1.3**) or with a mixture of Si-PEG$_{1k}$ and TEPSA–TEMPO (SNP **2.1–2.2**).

nitroxide concentration was deduced from the maximum absorption band at 242 nm. ^{1}H NMR spectra were acquired on a 500 MHz Bruker Avance II instrument (Bruker, Germany). For the particle suspensions, spectra were recorded at 25 °C in H_2O/D_2O (9/1) using a water ^{1}H NMR peak suppression sequence. Chemical shifts (δ) are reported in ppm, coupling constants J are given in Hz, and the following abbreviations were used for the resonance multiplicity: s for singlet, d for doublet, q for quadruplet, and m for multiplet. Prior to analyses, the radicals were reduced by the addition of 10 μL of phenylhydrazine. Mass spectra were acquired in positive mode by using a ZQ spectrometer (Waters, Manchester, UK) equipped with an ESI source (ESI$^{(+)}$–MS). Relaxometric properties of the aqueous suspension were determined at 37 °C (±0.1 °C). Both R_1 and R_2 were measured at 20 MHz (0.47 T) and 60 MHz (1.51 T) on Bruker Minispec mq-20 and mq-60 (Karlsruhe, Germany), respectively.

The relative error in relaxation time measurements was below 4%.[30] Relaxivities r_1 and r_2 (in mM^{-1} s^{-1}) were calculated using the following relation

$$r_i(B, T) = \frac{(R_i - R_i^{\mathrm{dia}})}{[\mathrm{nitroxide}]} \tag{1}$$

where $R_i = \frac{1}{T_i}$, R_i^{dia} is the diamagnetic relaxation contribution of water (0.283 s^{-1} at 37 °C), and [nitroxide] the nitroxide concentration (obtained by UV spectroscopy).

The radical stability under reducing conditions was evaluated by ^{1}H relaxometry. A volume (360 μL) of the SNP suspensions in PBS at pH 7.4 was prepared. An ascorbate solution in PBS (15 μL; 250 mM) was added to the SNP suspension, reaching a final ascorbate concentration of 10 mM. The evolution of the T_2 relaxation time was followed over time at 37 °C and 20 or 60 MHz.

The mean number of nitroxides per NP (d^{TEMPO}) was estimated based on the following experimental data: the NP radius, determined by TEM microscopy (D^{TEM}) and the mass of silica (m) obtained after drying 1 mL of colloidal suspension. By considering the volume of a spherical particle, the mass associated with a single particle

$$m_{\mathrm{NP}} = V_{\mathrm{NP}}\rho \tag{2}$$

and the bulk material density (ρ = 2.4 g cm^{-3} at 20 °C), the mass of a single NP (m_{NP}) in suspension was calculated. The number of NPs in the sample (n_{NP}) was determined using the following relation

$$n_{\mathrm{NP}} = \frac{m}{m_{\mathrm{NP}}} \tag{3}$$

By incorporating Avogadro number and the nitroxide concentration, the number of nitroxide per particle was then calculated

$$n_{\mathrm{rad}} = \frac{[\mathrm{nitroxide}]N_{\mathrm{A}}}{n_{\mathrm{NP}}} \tag{4}$$

and was normalized by the surface area

$$\frac{n_{\mathrm{rad}}}{4\pi r^2} \tag{5}$$

L-band EPR spectra and EPR phantom images were recorded by using an L-band Bruker CW ELEXSYS E540L spectrometer. The following parameters were used: microwave frequency: 1.105 × 10^9 Hz; amplitude modulation: 2.000 G; and frequency modulation: 50 kHz. The other parameters were optimized, depending on the sample. The samples were placed in glass capillaries of various diameters to estimate the image resolution. Images were reconstructed using a procedure with total variation regularization.[31] X-ray microtomographs: Micro-CT imaging was performed using an 1178 X-ray computed scanner (SkyScan, Kontich, Belgium) to visualize the inner-glass capillaries.

Spectrum simulations were performed using EasySpin (ver. 6.0.6) in MATLAB R2022a. Initially, the broad signal was simulated using the garlic function, which does not account for correlation time, and a large line width was applied to isolate this component. After the simulated broad signal was subtracted from the experimental spectrum, the remaining sharp signal was simulated using the chili function, which incorporates correlation time. This simulation corresponds to the so-called "sharp signal". The sharp signal was then subtracted from the raw spectrum, and the residual broad signal was resimulated using the chili function to determine the parameters corresponding to the "large signal".

RESULTS AND DISCUSSION

Synthesis and Characterization of Nitroxide-Modified SNPs. Nitroxide-modified SNPs were obtained using a reverse w/o microemulsion process,[32] using TEOS as the silica precursor (Figure 1). The process begins by preparing a reverse w/o microemulsion with a cyclohexane/hexanol/Triton X-100/water mixture in a 9:2:2:1 volume ratio. TEOS

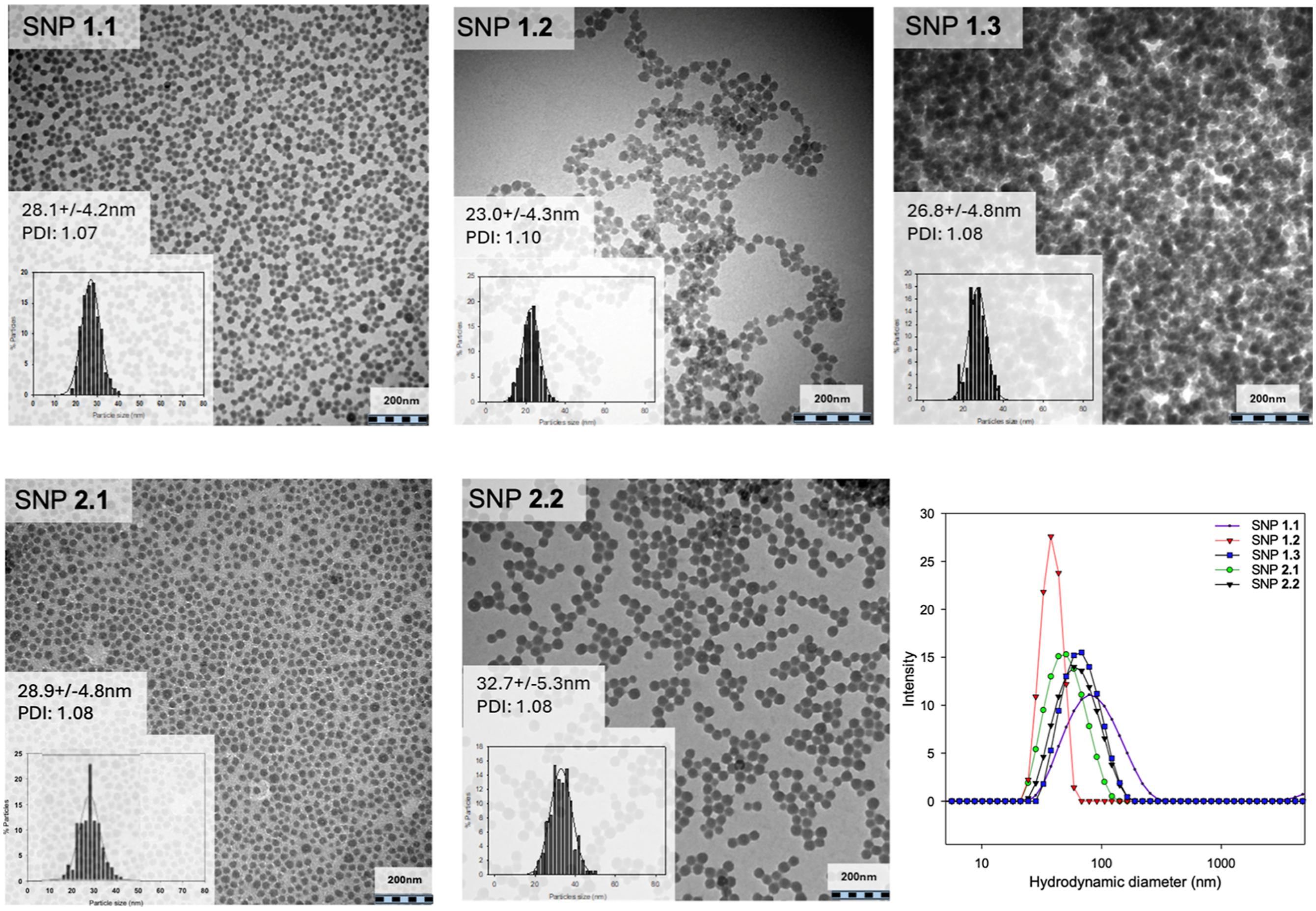

Figure 2. TEM images and corresponding size distributions obtained for the studied systems and their DLS intensity weighted size distribution (scale bar: 200 nm). The mean diameters D^{TEM} were estimated from several TEM images recorded for each triplicate.

Table 1. Physicochemical Properties of the Different Nitroxide-Modified SNPs; Relaxometric Measurements Were Performed at 37 °C

		relaxivities at 37 °C (mM^{-1} s^{-1})					
		20 MHz		60 MHz			
sample name	surface composition	r_1	r_2	r_1	r_2	d^{TEMPO} (n_{rad}/nm^2)	D^{TEM} (nm)
amino-TEMPO	_	0.17	0.21				
SNP 1.1	TEPSA−TEMPO	0.92	1.47	0.63	1.35	2.83	28.1 ± 4.2
SNP 1.2		0.92	1.84	0.61	1.82	1.46	22 ± 4.2
SNP 1.3		1.15	2.87	0.75	2.86	0.94	26.8 ± 4.6
SNP 2.1	TEPSA−TEMPO/PEG	2.35	5.69	1.51	5.53	0.56	28.9 ± 4.8
SNP 2.2		5.42	11.94	3.90	10.86	0.36	32.7 ± 5.3

was then added, followed by ammonia, to catalyze precursor hydrolysis and initiate polymerization. After a reactivation step, the particles were coated either with a TEMPO-modified silane (synthesized by reacting amino-TEMPO with TEPSA; SNP **1.1** to **1.3**) or with a mixture of TEMPO-silane and PEG-silane (SNP **2.1** and SNP **2.2**). For a fixed quantity of inorganic material, various amounts of coating agents were employed in order to induce variations in the overall radical surface densities.

By proceeding this way, spherical and monodisperse particles with average diameters ranging from ∼20 to ∼30 nm, as determined by TEM microscopy, were obtained (Figure 2). Colloidal stability in water was assessed via DLS, showing a narrow monomodal size distribution for all samples with an average hydrodynamic diameter (d_H) between 27 and 78 nm (Figure 2).

After purification through dialysis and ultrafiltration, surface modification was confirmed by using Fourier transform infrared (FTIR) and ^{1}H NMR. FTIR spectra (see Supporting Information, Figure S1) revealed characteristic bands of the SiO_2 matrix observed around 1100, 960, and 790 cm^{-1}, corresponding to Si−O−Si asymmetric stretching vibrations, Si−OH stretching, and Si−O−Si symmetric stretching, respectively. The grafting of the TEMPO derivative was confirmed by the appearance of C═O stretching (1716 cm^{-1}), N−O stretching (1550 cm^{-1}), C−H bending (1455 cm^{-1}), and C−H stretching around 2900 cm^{-1}. After treatment with phenylhydrazine to reduce paramagnetic radicals, ^{1}H NMR analysis (Figure S2) was performed and confirmed the surface

https://doi.org/10.1021/acs.langmuir.5c01616
Langmuir XXXX, XXX, XXX−XXX

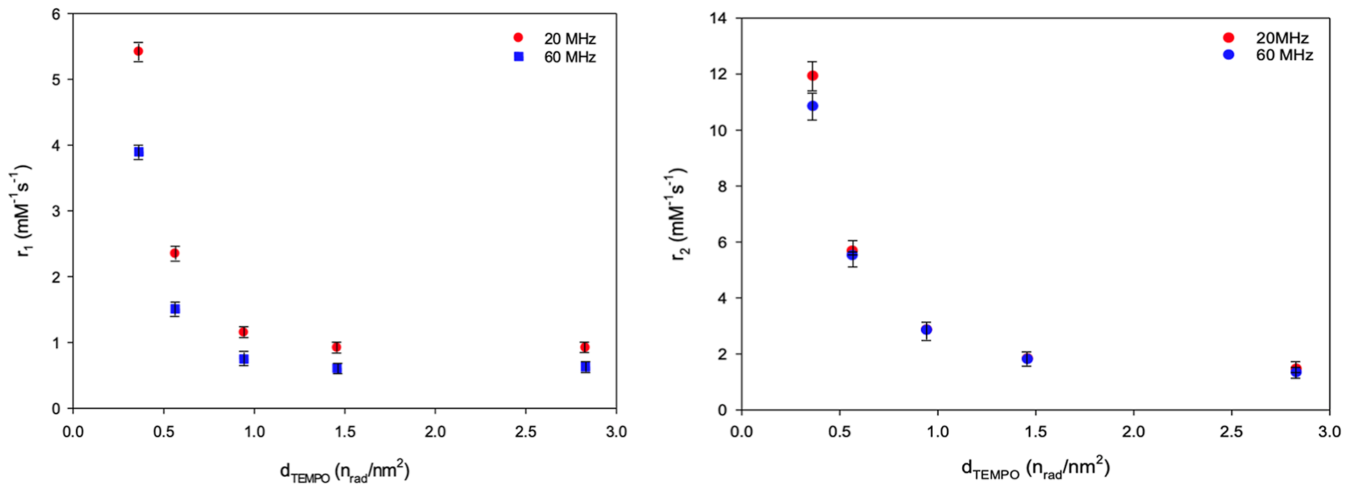

Figure 3. Plot of the relaxivities of particles versus their radical densities (20 and 60 MHz and 37 °C).

modification. Comparison of bare SNPs with TEPSA–TEMPO-treated particles showed the appearance of characteristic signals attributable to the methyl protons of the heterocycle (1.2, 1.95, and 4.1 ppm) and the propyl chain (0.6, 1.4, and 1.8 ppm). Concerning SNP **2** samples (i.e., PEGylated samples), additional signals at 3.6 and 3.3 ppm attributed to the protons of the methoxylated PEG chains confirmed the success of co-grafting.

The quantity of anchored nitroxides was determined by UV spectroscopy at 242 nm. As expected, our approach allowed for variation in radical density, with values ranging from 0.36 to 2.83 radicals/nm^2 (Table 1).

Evaluation of the Relaxometric Properties. TEMPO density variations significantly impacted the relaxometric performance of the NPs, with values at 20 MHz ranging from 0.92 to 5.42 $s^{-1}\cdot mM^{-1}$ for r_1 and from 1.47 to 11.94 $s^{-1}\cdot mM^{-1}$ for r_2. This corresponds to increases of approximately 489% and 712% for r_1 and r_2, respectively, compared to free amino-TEMPO (20 mM) for the least effective sample (SNP **1.1**). These findings indicate that despite their lower magnetic moment compared to that of Gd^{3+}, nitroxides such as TEMPO can still exhibit substantial relaxivity under optimal dynamic conditions. This behavior is closely linked to their molecular motion.[33−35] In aqueous solution, free radicals tumble rapidly (τ_R on the order of tens of picoseconds), a regime that poorly matches the Larmor frequency of protons and limits the efficiency of dipolar relaxation.[36−39] Upon tethering to larger structures such as SNPs, the rotational motion of nitroxides is strongly hindered, increasing τ_R to several nanoseconds. This slowing down brings the modulation of the dipolar interaction into a regime that is more favorable for outer sphere relaxation. Notably, this rotational restriction is often accompanied by an increase in the electron spin relaxation time (τ_{Si}), which typically reaches values around 500 ns in fast-tumbling systems (at room temperature and moderate magnetic fields, ≥350 mT),[36−39] and extends to a few microseconds when motion is restricted, such as in viscous media or when tethered to large structures[33−35] (for comparison, the electronic spin relaxation time for gadolinium is on the order of 10^{-8} seconds[40]). Together, these changes facilitate more efficient proton relaxation through dipolar coupling.

In addition, one may suggest that anchoring nitroxides to hydrophilic surfaces such as silica may prolong the residence time of water molecules near the paramagnetic sites, effectively increasing the translational correlation time. This sustained interaction further enhances dipolar relaxation pathways and contributes to the observed increase in the r_1 and r_2 values.

At first glance, one might expect a higher radical density to correlate with higher proton relaxivity, given the greater number of unpaired electrons. Interestingly, it can be noticed that increasing radical density on the particle surface has a negative impact on both observed relaxivity values (Figure 3). Similar observations were made at a higher magnetic field.

We hypothesize that the decrease in relaxivity observed at high nitroxide densities arises from strong spin−spin interactions between neighboring radicals.[34,41] At high TEMPO densities, the reduced average distance between nitroxides likely leads to enhanced dipolar and exchange interactions between radical electron spins. These interactions shorten the electron relaxation times, thereby diminishing the efficiency of the dipolar coupling between the unpaired electron and nearby water protons and thus reducing relaxivity. Thus, optimal nitroxide relaxivity is achieved when radicals are sufficiently isolated to minimize spin−spin interactions while still benefiting from the local chemical environment and restricted rotational mobility provided by NP immobilization. In this context, PEGylation plays a crucial role, as the PEG chains help maintain spatial separation between individual TEMPO moieties, effectively limiting detrimental inter-radical interactions. This spatial isolation contributes to keeping longer electron relaxation times, thereby enhancing relaxivity. This behavior is well documented in EPR studies, where strong interspin interactions are known to reduce radical relaxivity performance.

EPR Spectroscopy and Imaging. To investigate the effect of inter-radical proximity on EPR spectral characteristics, L-band EPR spectroscopy (Figure 4) was performed on two samples with markedly different TEMPO densities, SNP **1.1** and SNP **2.1**. The spectrum of the sample with lower radical density (SNP **2.1**) displayed the characteristic nitroxide triplet (Figure 4), though the intensity of the third peak was diminished, likely due to reduced nitroxide mobility following grafting onto the NP surface.[42] In contrast, the spectrum of the higher-density sample (SNP **1.1**) showed notable deviations, including a steeper slope and broader signal base, indicative of enhanced spin−spin interactions.[43] A distinct increase in signal width was observed for SNP **1.1** compared to SNP **2.1**, with peak-to-peak distances of 0.252 and 0.220 mT, respectively.

https://doi.org/10.1021/acs.langmuir.5c01616
Langmuir XXXX, XXX, XXX−XXX

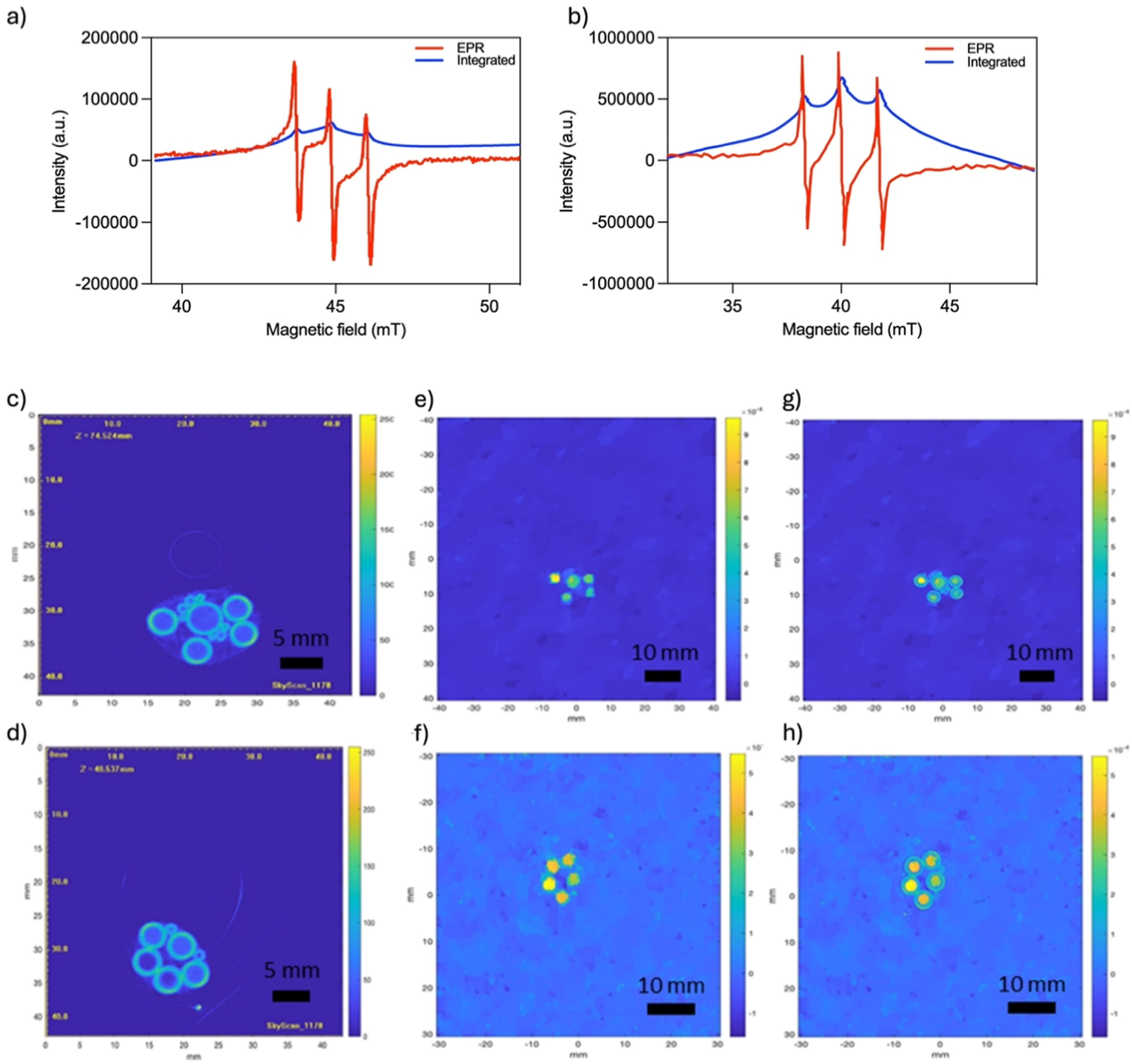

Figure 4. L-band EPR spectra of (a) SNP-TEMPO (SNP **1.1**) and (b) SNP-TEMPO-PEG (SNP **2.1**). (c,d) Micro-CT anatomic 2D images of the glass capillaries used to image SNP **1.1** and SNP **2.1**, respectively; (e,f) reconstruction EPRI image obtained from SNP **1.1** and SNP **2.1**, respectively; and (g,h) superimposition of the micro-CT image and the corresponding EPR image obtained from SNP **1.1** and SNP **2.1**, respectively.

These differences became even more pronounced upon integration of the spectra, revealing two distinct nitroxide populations: a broad signal superimposed on the expected triplet. The broader component likely corresponds to radicals in densely packed regions, where stronger interspin interactions prevail, whereas the sharper triplet could be attributed to more isolated radicals (Figure 4b).

The data obtained by fitting the experimental results appear to support this hypothesis (see Supporting Information, Table S1), suggesting that the two populations detected by EPR may correspond to distinct localizations of radicals within the NPs. This interpretation is plausible if we assume that these SNPs exhibit a certain degree of porosity. The "broad" spectral component, characterized by a longer correlation time (25 ns for SNP **1.1** and 100 ns for SNP **2.1**), likely corresponds to radicals embedded or confined within the pores, where restricted mobility and close proximity favor dipolar interactions. In contrast, the "sharp" component, with correlation times on the order of nanoseconds, is attributed to more mobile radicals located on the particle surface, where increased spatial separation maintains higher mobility and rotational freedom.

This hypothesis is further substantiated by structural characterization data. Although designed to be solid and nonporous, nitrogen adsorption/desorption isotherms (Figure 5a) suggest the presence of mesopores between 2 and 4 nm in diameter.[44] A comparison of specific surface area (SSA) between radical-functionalized and nonfunctionalized particles supports this interpretation, with SSA decreasing significantly from 195 m^2/g to 124.2 m^2/g following surface modification,

https://doi.org/10.1021/acs.langmuir.5c01616
Langmuir XXXX, XXX, XXX−XXX

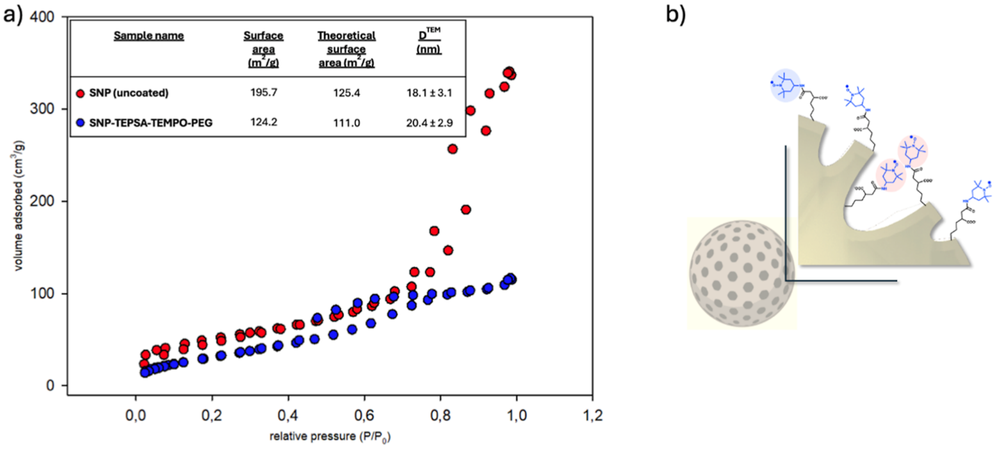

Figure 5. (a) BET isotherm plots from uncoated (red dots) and TEMPO-modified SNP (blue dots) prepared by the microemulsion process and (b) schematic representations of the rugosity of the SNP showing that the proximity of the radicals increases inside the pores.

approaching the theoretical SSA for solid particles of this size (∼111 m^2/g). These findings reinforce the notion of structural heterogeneity in radical distribution, governed by the surface architecture of the NPs, with some radicals being confined within mesopores, where restricted mobility and close proximity enhance spin−spin interactions (Figure 5b), while others are located on the external surface, exhibiting greater freedom and weaker interactions.

To assess whether the observed spectral differences impacted EPRI sensitivity, phantom images were acquired using samples placed in glass tubes of varying diameters: one 3.5 mm tube, four 2.7 mm tubes, and smaller capillaries ranging from 0.7 to 0.3 mm. Image reconstruction was performed using an advanced algorithm incorporating total variation regularization, developed by Abergel et al.[31] For the SNP **1.1** sample, only the larger tubes (3.5 and 2.7 mm) were visible in the reconstructed images. In contrast, the SNP **2.1** sample enabled the visualization of smaller capillaries, down to 0.7 mm in diameter, demonstrating superior spatial resolution. Finally, overlaying the EPR phantom images with a CT scan of the glass tubes confirmed that the shape and position of the EPR signals accurately matched the original tube geometry (Figure 4c−h).

Radical Stability Evaluation. Nitroxide chemical stability was evaluated by monitoring T_2 relaxation at 20 MHz over time in a 10 mM ascorbate solution. Upon reduction to diamagnetic hydroxylamines, the radicals lose their paramagnetic properties, leading to a decrease in ^{1}H relaxivity (Figure 6). Under these conditions, free amino-TEMPO ([TEMPO] = 20 mM) showed rapid reduction with a half-life ($t_1/_2$) of 17.3 s, indicating low stability. In contrast, when radicals were grafted onto the surface of PEGylated SNPs (SNPs), a plateau was reached after approximately 10 min, resulting in a significantly extended $t_1/_2$ of 105.5 s. This enhanced stability is likely due to steric hindrance provided by the PEG chains, which shield the radicals from reducing agents.

The specific contribution of PEG to chemical stabilization could not be fully isolated, as non-PEGylated particles exhibited poor colloidal stability and precipitated rapidly upon dilution in the test medium. Nevertheless, co-grafting TEPSA−TEMPO and PEG markedly improved resistance to reduction compared to free nitroxides, although the resulting stability was still lower than typically reported for nano-

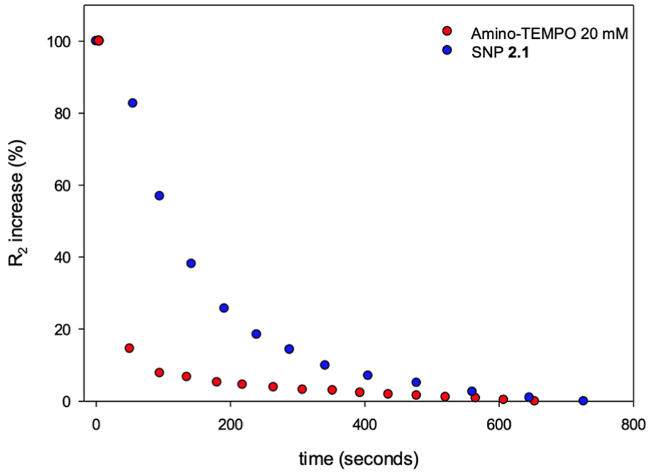

Figure 6. Evolution of the transverse relaxation rate (R_2) against time of amino-TEMPO (red dots) and SNP **2.1** (blue dots) in 10 mM ascorbate solution (PBS, pH 7.4, T°: 37 °C).

particulate nitroxides, which may be seen as suboptimal. To further improve the stability, we explored radical encapsulation within the NP matrix. This strategy significantly increased $t_1/_2$ values—from 105.5 s for surface-bound radicals to several hours (Figure S3), demonstrating effective protection in reducing environments. However, as anticipated, this approach resulted in significant signal broadening (data not shown), highlighting a trade-off between radical stability and EPR signal resolution.

■ CONCLUSIONS

Due to their paramagnetic properties, nitroxides have the potential to be used as MRI contrast agents, offering an alternative to gadolinium-based compounds. However, compared to GBCAs, their relaxivity is significantly lower, which is partly due to the relaxation mechanisms of free nitroxide radicals, primarily involving outer sphere interactions. Recent studies[18,21,45] have suggested that incorporating nitroxides within nanosystems can greatly enhance their proton relaxivity and improve radical stability, positioning these metal-free NP systems as promising candidates for generating strong and long-lasting signals in vivo. When these systems are compared, significant variations in their relaxivities are observed with a

https://doi.org/10.1021/acs.langmuir.5c01616
Langmuir XXXX, XXX, XXX−XXX

strong dependence on structure. While NP chemical composition is crucial in determining these properties, several studies highlight the importance of dynamic parameters in enhancing radical relaxivity.[46,47] In this context, silica was selected as the primary material due to its favorable properties and versatile chemistry. This versatility enables precise tuning of the radical microenvironment, such as polarity, water diffusion, radical proximity, and mobility, all of which impact the overall relaxation behavior.

Monodisperse SNPs with varying surface radical densities were synthesized by using the microemulsion method. As anticipated, TEMPO functionalization enhanced both longitudinal and transverse relaxivities compared to free amino-TEMPO. Notably, lower nitroxide surface densities led to significantly higher relaxivity values, an important observation for the future development of nitroxide-based NP contrast agents. This effect is likely due to reduced spin−spin interactions between neighboring radicals, which can otherwise lead to a relaxivity decrease.

While large NP doses (several tens of milligrams) are typically required to achieve measurable relaxation time reductions in MRI applications, SNPs with optimized radical density may be better suited for EPRI, where lower radical densities enhance spatial resolution. Beyond sensitivity, nitroxide stability in reducing environments remains crucial. Co-grafting TEPSA−TEMPO and PEG significantly improved radical stability against ascorbate reduction compared to free nitroxides, likely due to steric protection from PEG chains. However, this stabilization is still less pronounced than that commonly reported for other nanoparticulate nitroxides, which may be considered suboptimal.

Overall, this study demonstrates that tuning nitroxide density and NP design can markedly improve proton relaxivity and radical stability—both critical for imaging probe performance. Further exploration of alternative encapsulation strategies or coatings may address chemical stability challenges while minimizing adverse effects on EPR signal quality.

■ ASSOCIATED CONTENT

Supporting Information

The Supporting Information is available free of charge at https://pubs.acs.org/doi/10.1021/acs.langmuir.5c01616.

FTIR characterization, ^{1}H NMR spectra, radical stability evaluation, and EPR simulation results for two signal components (PDF)

■ AUTHOR INFORMATION

Corresponding Author

Dimitri Stanicki − *NMR and Molecular Imaging Laboratory, General, Organic and Biomedical Chemistry Unit, University of Mons, B-7000 Mons, Belgium*; Phone: +32-65373594; Email: dimitri.stanicki@umons.ac.be

Authors

Pierre Ernotte − *NMR and Molecular Imaging Laboratory, General, Organic and Biomedical Chemistry Unit, University of Mons, B-7000 Mons, Belgium*

Amandine Maes − *NMR and Molecular Imaging Laboratory, General, Organic and Biomedical Chemistry Unit, University of Mons, B-7000 Mons, Belgium*; orcid.org/0009-0003-4665-5512

Sarah Garifo − *NMR and Molecular Imaging Laboratory, General, Organic and Biomedical Chemistry Unit, University of Mons, B-7000 Mons, Belgium*; orcid.org/0000-0003-1137-7690

Isalyne Drewek − *NMR and Molecular Imaging Laboratory, General, Organic and Biomedical Chemistry Unit, University of Mons, B-7000 Mons, Belgium*

Yves-Michel Frapart − *University of Paris Cité, LCBPT, F-75006 Paris, France*

Robert N. Muller − *NMR and Molecular Imaging Laboratory, General, Organic and Biomedical Chemistry Unit, University of Mons, B-7000 Mons, Belgium; Center for Microscopy and Molecular Imaging (CMMI), B-6041 Gosselies, Belgium*

Sophie Laurent − *NMR and Molecular Imaging Laboratory, General, Organic and Biomedical Chemistry Unit, University of Mons, B-7000 Mons, Belgium; Center for Microscopy and Molecular Imaging (CMMI), B-6041 Gosselies, Belgium*

Complete contact information is available at: https://pubs.acs.org/10.1021/acs.langmuir.5c01616

Notes

The authors declare no competing financial interest.

■ ACKNOWLEDGMENTS

The authors thank the Center for Microscopy and Molecular Imaging (CMMI, supported by the European Regional Development Fund and the Walloon Region). This work was supported by the Fond National de la Recherche Scientifique (FNRS), the ARC Programs of the French Community of Belgium, and the Walloon Region (Prother-Wal and Interreg projects).

■ REFERENCES

(1) Xiao, Y.-D.; Paudel, R.; Liu, J.; Ma, C.; Zhang, Z.-S.; Zhou, S.-K. MRI Contrast Agents: Classification and Application. *Int. J. Mol. Med.* **2016**, *38* (5), 1319−1326.

(2) Pasquini, L.; Napolitano, A.; Visconti, E.; Longo, D.; Romano, A.; Tomà, P.; Espagnet, M. C. R. Gadolinium-Based Contrast Agent-Related Toxicities. *CNS Drugs* **2018**, *32* (3), 229−240.

(3) Roberts, D. R.; Holden, K. R. Progressive Increase of T1 Signal Intensity in the Dentate Nucleus and Globus Pallidus on Unenhanced T1-Weighted MR Images in the Pediatric Brain Exposed to Multiple Doses of Gadolinium Contrast. *Brain Dev.* **2016**, *38* (3), 331−336.

(4) Vangijzegem, T.; Stanicki, D.; Panepinto, A.; Socoliuc, V.; Vekas, L.; Muller, R. N.; Laurent, S. Influence of Experimental Parameters of a Continuous Flow Process on the Properties of Very Small Iron Oxide Nanoparticles (VSION) Designed for T1-Weighted Magnetic Resonance Imaging (MRI). *Nanomaterials* **2020**, *10* (4), 757.

(5) Gossuin, Y.; Martin, E.; Vuong, Q. L.; Delroisse, J.; Laurent, S.; Stanicki, D.; Rousseau, C. Characterization of Commercial Iron Oxide Clusters with High Transverse Relaxivity. *J. Magn. Reson. Open* **2022**, *10−11*, 100054.

(6) Lewandowski, M.; Gwozdzinski, K. Nitroxides as Antioxidants and Anticancer Drugs. *Int. J. Mol. Sci.* **2017**, *18* (11), 2490.

(7) Genovese, D.; Baschieri, A.; Vona, D.; Baboi, R. E.; Mollica, F.; Prodi, L.; Amorati, R.; Zaccheroni, N. Nitroxides as Building Blocks for Nanoantioxidants. *ACS Appl. Mater. Interfaces* **2021**, *13* (27), 31996−32004.

(8) Torricella, F.; Pierro, A.; Mileo, E.; Belle, V.; Bonucci, A. Nitroxide Spin Labels and EPR Spectroscopy: A Powerful Association for Protein Dynamics Studies. *Biochim. Biophys. Acta, Proteins Proteomics* **2021**, *1869* (7), 140653.

(9) Wahsner, J.; Gale, E. M.; Rodríguez-Rodríguez, A.; Caravan, P. Chemistry of MRI Contrast Agents: Current Challenges and New Frontiers. *Chem. Rev.* **2019**, *119* (2), 957−1057.

(10) Soule, B.; Hyodo, F.; Matsumoto, K.; Simone, N.; Cook, J.; Krishna, M.; Mitchell, J. The Chemistry and Biology of Nitroxide Compounds. *Free Radic. Biol. Med.* **2007**, *42* (11), 1632−1650.

(11) Akakuru, O. U.; Iqbal, M. Z.; Saeed, M.; Liu, C.; Paunesku, T.; Woloschak, G.; Hosmane, N. S.; Wu, A. The Transition from Metal-Based to Metal-Free Contrast Agents for T_1 Magnetic Resonance Imaging Enhancement. *Bioconjugate Chem.* **2019**, *30* (9), 2264−2286.

(12) Couet, W. R.; Brasch, R. C.; Sosnovsky, G.; Tozer, T. N. Factors Affecting Nitroxide Reduction in Ascorbate Solution and Tissue Homogenates. *Magn. Reson. Imaging* **1985**, *3* (1), 83−88.

(13) Pinto, L. F.; Lloveras, V.; Zhang, S.; Liko, F.; Veciana, J.; Muñoz-Gómez, J. L.; Vidal-Gancedo, J. Fully Water-Soluble Polyphosphorhydrazone-Based Radical Dendrimers Functionalized with Tyr-PROXYL Radicals as Metal-Free MRI T_1 Contrast Agents. *ACS Appl. Bio Mater.* **2020**, *3* (1), 369−376.

(14) Xia, L.; Zhang, C.; Li, M.; Wang, K.; Wang, Y.; Xu, P.; Hu, Y. Nitroxide-Radicals−Modified Gold Nanorods for in Vivo CT/MRI-Guided Photothermal Cancer Therapy. *Int. J. Nanomed.* **2018**, *13*, 7123−7134.

(15) Nagura, K.; Bogdanov, A.; Chumakova, N.; Vorobiev, A. K.; Moronaga, S.; Imai, H.; Matsuda, T.; Noda, Y.; Maeda, T.; Koizumi, S.; Sakamoto, K.; Amano, T.; Yoshino, F.; Kato, T.; Komatsu, N.; Tamura, R. Size-Tunable MRI-Visible Nitroxide-Based Magnetic Mixed Micelles: Preparation, Stability, and Theranostic Application. *Nanotechnology* **2019**, *30* (22), 224002.

(16) Nagura, K.; Takemoto, Y.; Yoshino, F.; Bogdanov, A.; Chumakova, N.; Vorobiev, A.; Imai, H.; Matsuda, T.; Shimono, S.; Kato, T.; Komatsu, N.; Tamura, R. Magnetic Mixed Micelles Composed of a Non-Ionic Surfactant and Nitroxide Radicals Containing a D-Glucosamine Unit: Preparation, Stability, and Biomedical Application. *Pharmaceutics* **2019**, *11* (1), 42.

(17) Dobrynin, S.; Kutseikin, S.; Morozov, D.; Krumkacheva, O.; Spitsyna, A.; Gatilov, Y.; Silnikov, V.; Angelovski, G.; Bowman, M. K.; Kirilyuk, I.; Chubarov, A. Human Serum Albumin Labelled with Sterically-Hindered Nitroxides as Potential MRI Contrast Agents. *Molecules* **2020**, *25* (7), 1709.

(18) Guo, S.; Wang, X.; Li, Z.; Pan, D.; Dai, Y.; Ye, Y.; Tian, X.; Gu, Z.; Gong, Q.; Zhang, H.; Luo, K. A Nitroxides-Based Macromolecular MRI Contrast Agent with an Extraordinary Longitudinal Relaxivity for Tumor Imaging via Clinical T1WI SE Sequence. *J. Nanobiotechnol.* **2021**, *19* (1), 244.

(19) Muir, B. W.; Acharya, D. P.; Kennedy, D. F.; Mulet, X.; Evans, R. A.; Pereira, S. M.; Wark, K. L.; Boyd, B. J.; Nguyen, T.-H.; Hinton, T. M.; Waddington, L. J.; Kirby, N.; Wright, D. K.; Wang, H. X.; Egan, G. F.; Moffat, B. A. Metal-Free and MRI Visible Theranostic Lyotropic Liquid Crystal Nitroxide-Based Nanoparticles. *Biomaterials* **2012**, *33* (9), 2723−2733.

(20) Nguyen, H. V.-T.; Chen, Q.; Paletta, J. T.; Harvey, P.; Jiang, Y.; Zhang, H.; Boska, M. D.; Ottaviani, M. F.; Jasanoff, A.; Rajca, A.; Johnson, J. A. Nitroxide-Based Macromolecular Contrast Agents with Unprecedented Transverse Relaxivity and Stability for Magnetic Resonance Imaging of Tumors. *ACS Cent. Sci.* **2017**, *3* (7), 800−811.

(21) Akakuru, O. U.; Xu, C.; Liu, C.; Li, Z.; Xing, J.; Pan, C.; Li, Y.; Nosike, E. I.; Zhang, Z.; Iqbal, Z. M.; Zheng, J.; Wu, A. Metal-Free Organo-Theranostic Nanosystem with High Nitroxide Stability and Loading for Image-Guided Targeted Tumor Therapy. *ACS Nano* **2021**, *15* (2), 3079−3097.

(22) Huang, Y.; Li, P.; Zhao, R.; Zhao, L.; Liu, J.; Peng, S.; Fu, X.; Wang, X.; Luo, R.; Wang, R.; Zhang, Z. Silica Nanoparticles: Biomedical Applications and Toxicity. *Biomed. Pharmacother.* **2022**, *151*, 113053.

(23) Bitar, A.; Ahmad, N. M.; Fessi, H.; Elaissari, A. Silica-Based Nanoparticles for Biomedical Applications. *Drug Discovery Today* **2012**, *17* (19−20), 1147−1154.

(24) Lipani, E.; Laurent, S.; Surin, M.; Elst, L. V.; Leclère, P.; Muller, R. N. High-Relaxivity and Luminescent Silica Nanoparticles As Multimodal Agents for Molecular Imaging. *Langmuir* **2013**, *29* (10), 3419−3427.

(25) Lechevallier, S.; Mauricot, R.; Gros-Dagnac, H.; Chevreux, S.; Lemercier, G.; Phonesouk, E.; Golzio, M.; Verelst, M. Silica-Based Nanoparticles as Bifunctional and Bimodal Imaging Contrast Agents. *ChemPlusChem* **2017**, *82* (5), 770−777.

(26) Garifo, S.; Stanicki, D.; Boutry, S.; Larbanoix, L.; Ternad, I.; Muller, R. N.; Laurent, S. Functionalized Silica Nanoplatform as a Bimodal Contrast Agent for MRI and Optical Imaging. *Nanoscale* **2021**, *13* (39), 16509−16524.

(27) Fedorenko, S. V.; Grechkina, S. L.; Mustafina, A. R.; Kholin, K. V.; Stepanov, A. S.; Nizameev, I. R.; Ismaev, I. E.; Kadirov, M. K.; Zairov, R. R.; Fattakhova, A. N.; Amirov, R. R.; Soloveva, S. E. Tuning the Non-Covalent Confinement of Gd(III) Complexes in Silica Nanoparticles for High T1-Weighted MR Imaging Capability. *Colloids Surf. B Biointerfaces* **2017**, *149*, 243−249.

(28) Krzyminiewski, R.; Kubiak, T.; Dobosz, B.; Schroeder, G.; Kurczewska, J. EPR Spectroscopy and Imaging of TEMPO-Labeled Magnetite Nanoparticles. *Curr. Appl. Phys.* **2014**, *14* (5), 798−804.

(29) Hannecart, A.; Stanicki, D.; Elst, L. V.; Muller, R. N.; Brûlet, A.; Sandre, O.; Schatz, C.; Lecommandoux, S.; Laurent, S. Embedding of Superparamagnetic Iron Oxide Nanoparticles into Membranes of Well-Defined Poly(Ethylene Oxide)- *Block* -Poly(ε-Caprolactone) Nanoscale Magnetovesicles as Ultrasensitive MRI Probes of Membrane Bio-Degradation. *J. Mater. Chem. B* **2019**, *7* (30), 4692−4705.

(30) Bernardi, M.; Hantson, A.-L.; Caulier, G.; Eyley, S.; Thielemans, W.; De Weireld, G.; Gossuin, Y. Ni2+ Removal by Ion Exchange Resins and Activated Carbon: A Benchtop NMR Study. *Int. J. Environ. Sci. Technol.* **2024**, *21* (13), 8337−8360.

(31) Abergel, R.; Boussâa, M.; Durand, S.; Frapart, Y.-M. Electron Paramagnetic Resonance Image Reconstruction with Total Variation Regularization. *Image Process. On Line* **2023**, *13*, 90−139.

(32) Finnie, K. S.; Bartlett, J. R.; Barbé, C. J. A.; Kong, L. Formation of Silica Nanoparticles in Microemulsions. *Langmuir* **2007**, *23* (6), 3017−3024.

(33) Sato, H.; Kathirvelu, V.; Fielding, A.; Blinco, J. P.; Micallef, A. S.; Bottle, S. E.; Eaton, S. S.; Eaton, G. R. Impact of Molecular Size on Electron Spin Relaxation Rates of Nitroxyl Radicals in Glassy Solvents between 100 and 300 K. *Mol. Phys.* **2007**, *105* (15−16), 2137−2151.

(34) Sato, H.; Bottle, S. E.; Blinco, J. P.; Micallef, A. S.; Eaton, G. R.; Eaton, S. S. Electron Spin−Lattice Relaxation of Nitroxyl Radicals in Temperature Ranges That Span Glassy Solutions to Low-Viscosity Liquids. *J. Magn. Reson.* **2008**, *191* (1), 66−77.

(35) Sato, H.; Kathirvelu, V.; Spagnol, G.; Rajca, S.; Rajca, A.; Eaton, S. S.; Eaton, G. R. Impact of Electron−Electron Spin Interaction on Electron Spin Relaxation of Nitroxide Diradicals and Tetraradical in Glassy Solvents Between 10 and 300 K. *J. Phys. Chem. B* **2008**, *112* (10), 2818−2828.

(36) Biller, J. R.; Meyer, V.; Elajaili, H.; Rosen, G. M.; Kao, J. P. Y.; Eaton, S. S.; Eaton, G. R. Relaxation Times and Line Widths of Isotopically-Substituted Nitroxides in Aqueous Solution at X-Band. *J. Magn. Reson.* **2011**, *212* (2), 370−377.

(37) Biller, J. R.; Meyer, V. M.; Elajaili, H.; Rosen, G. M.; Eaton, S. S.; Eaton, G. R. Frequency Dependence of Electron Spin Relaxation Times in Aqueous Solution for a Nitronyl Nitroxide Radical and Perdeuterated-Tempone between 250 MHz and 34 GHz. *J. Magn. Reson.* **2012**, *225*, 52−57.

(38) Biller, J. R.; Elajaili, H.; Meyer, V.; Rosen, G. M.; Eaton, S. S.; Eaton, G. R. Electron Spin−Lattice Relaxation Mechanisms of Rapidly-Tumbling Nitroxide Radicals. *J. Magn. Reson.* **2013**, *236*, 47−56.

(39) Martin, R. M.; Diaz, S.; Poncelet, M.; Driesschaert, B.; Barth, E.; Kotecha, M.; Epel, B.; Eaton, G. R.; Biller, J. R. Toward a Nanoencapsulated EPR Imaging Agent for Clinical Use. *Mol. Imaging Biol.* **2024**, *26* (3), 525−541.

(40) Scarciglia, A.; Papi, C.; Romiti, C.; Leone, A.; Di Gregorio, E.; Ferrauto, G. Gadolinium-Based Contrast Agents (GBCAs) for MRI:

A Benefit−Risk Balance Analysis from a Chemical, Biomedical, and Environmental Point of View. *Glob. Chall.* **2025**, *9* (3), 2400269.

(41) Moore, W.; Yao, R.; Liu, Y.; Eaton, S. S.; Eaton, G. R. Spin-Spin Interaction and Relaxation in Two Trityl-Nitroxide Diradicals. *J. Magn. Reson.* **2021**, *332*, 107078.

(42) Zubanova, E. M.; Ivanova, T. A.; Ksendzov, E. A.; Kostjuk, S. V.; Timashev, P. S.; Melnikov, M. Ya.; Golubeva, E. N. Structure and Dynamics of Inhomogeneities in Aqueous Solutions of Graft Copolymers of N-Isopropylacrylamide with Lactide (P(NIPAM-Graft-PLA)) by Spin Probe EPR Spectroscopy. *Polymers* **2022**, *14* (21), 4746.

(43) Kaim, A.; Szydłowska, J.; Piotrowski, P.; Megiel, E. One-Pot Synthesis of Gold Nanoparticles Densely Coated with Nitroxide Spins. *Polyhedron* **2012**, *46* (1), 119−123.

(44) Cueto-Díaz, E. J.; Castro-Muñiz, A.; Suárez-García, F.; Gálvez-Martínez, S.; Torquemada-Vico, M. C.; Valles-González, M. P.; Mateo-Martí, E. APTES-Based Silica Nanoparticles as a Potential Modifier for the Selective Sequestration of CO2 Gas Molecules. *Nanomaterials* **2021**, *11* (11), 2893.

(45) Nguyen, H. V.-T.; Detappe, A.; Gallagher, N. M.; Zhang, H.; Harvey, P.; Yan, C.; Mathieu, C.; Golder, M. R.; Jiang, Y.; Ottaviani, M. F.; Jasanoff, A.; Rajca, A.; Ghobrial, I.; Ghoroghchian, P. P.; Johnson, J. A. Triply Loaded Nitroxide Brush-Arm Star Polymers Enable Metal-Free Millimetric Tumor Detection by Magnetic Resonance Imaging. *ACS Nano* **2018**, *12* (11), 11343−11354.

(46) Vallet, P.; Van Haverbeke, Y.; Bonnet, P. A.; Subra, G.; Chapat, J.-P.; Muller, R. N. Relaxivity Enhancement of Low Molecular Weight Nitroxide Stable Free Radicals: Importance of Structure and Medium. *Magn. Reson. Med.* **1994**, *32* (1), 11−15.

(47) Bennett, H. F.; Brown, R. D.; Koenig, S. H.; Swartz, H. M. Effects of Nitroxides on the Magnetic Field and Temperature Dependence of 1/T1 of Solvent Water Protons. *Magn. Reson. Med.* **1987**, *4* (2), 93−111.

https://doi.org/10.1021/acs.langmuir.5c01616
Langmuir XXXX, XXX, XXX−XXX